A New Nickel(III) Oxide Family: MSr_3NiO_6 (M = Sc, In, Tm, Yb and Lu)

Michael James and J. Paul Attfield*

Abstract: The new phases $M^{III}Sr_3Ni^{III}O_6$ have been prepared for M = Sc, In, Tm, Yb and Lu. Thermogravimetric analysis indicates that these phases are stoichiometric nickel(III) oxides. Rietveld refinement of their crystal structures from powder X-ray diffraction data confirms that they adopt the rhombohedral K_4CdCl_6-type structure (space group $R\bar{3}c$, $a = 9.6595(2)$ and $c = 10.8546(3)$ Å for $ScSr_3NiO_6$). The M site is fully occupied for M = Sc and In, but a deficiency of scattering for M = Tm, Yb and Lu is shown to be due to Ni substitution through a simultaneous refinement of the $YbSr_3NiO_6$ structure using X-ray and time-of-flight neutron diffraction data. The refined composition is $(Yb_{0.83}Ni_{0.17})$-Sr_3NiO_6. The magnetic susceptibilities of the M = Sc, In and Lu samples show Curie–Weiss behaviour down to 6 K; however, $ScSr_3NiO_6$ shows a broad transition between 250 and 290 K, with Curie–Weiss behaviour above and below this anomaly. This transition is thought to be between the statically and dynamically Jahn–Teller distorted regimes of octahedrally coordinated, low-spin Ni^{3+}.

Keywords
Jahn–Teller distortions · magnetic properties · neutron powder diffraction · nickel oxides · X-ray powder diffraction

Introduction

Nickel(III) oxides are of interest for their "high" oxidation state and for their structural, magnetic and electronic properties in relation to high Tc superconductors, as both low spin Ni^{3+} and Cu^{2+} have $S = {}^1/_2$ ground states. The three-dimensional perovskites $LnNiO_3$ (Ln = La–Gd)[1–3] and layered K_2NiF_4-type $Ln_{2-x}Sr_xNiO_{4-\delta}$ solid solutions (Ln = La,[4–6] Nd,[7–9] Pr, Sm and Gd)[9, 10] have been extensively studied. We have recently prepared a series of related Ni^{III} defect oxides $Ln_{0.33}Sr_{1.67}NiO_{3.67}$ ($LnSr_5Ni_3O_{11}$) for Ln = Y, Dy, Ho, Er and Tm.[11, 12] Attempts to prepare the Yb analogue of these phases resulted in the formation of a new rhombohedral Ni^{III} compound $YbSr_3NiO_6$, for which preliminary results have been reported.[13] This paper describes further results for $YbSr_3NiO_6$ and the preparation and characterisation of the family of isostructural phases MSr_3NiO_6 (M = Sc, In, Tm and Lu).

Results

Powder X-ray diffraction profiles were recorded for each of the new phases. It was found that the major phase in each case for M = Sc, In, Tm, Yb and Lu could be indexed on a rhombohedral unit cell with hexagonal lattice parameters similar to those of K_4CdCl_6-type oxides such as Sr_4PtO_6.[14, 15] Small quantities of M_2SrO_4 phases[16–18] were observed for M = Tm, Yb and Lu, and SrO was found in all of the samples containing the rhombohedral phase, with the exception of $InSr_3NiO_6$, which was phase-pure by powder X-ray diffraction. The indexed pattern of $InSr_3NiO_6$ is given in Table 1. The rhombohedral phase was not observed for M = Ga, which gave a mixture of phases including $Sr_5Ni_4O_{11}$,[19] $Sr_3Ga_2O_6$,[20] NiO and SrO, or for M = Er, which gave $ErSr_5Ni_3O_{11}$,[12] Er_2SrO_4[16] and SrO.

Table 1. Observed d spacings and relative peak intensities (I_r) for X-ray diffraction pattern of $InSr_3NiO_6$.

hkl	d spacing (Å)	I_r	hkl	d spacing (Å)	I_r
110	4.787	15	223	2.014	23
102	4.620	1	321	1.883	2
202	3.320	13	006	1.847	7
211	3.022	4	410	1.842	4
113	2.923	48	215	1.818	4
300	2.772	100	322	1.807	11
212	2.733	8	314	1.773	3
104	2.624	3	116	1.722	1
204	2.303	19	404	1.667	1
311	2.260	17	413	1.630	5
312	2.134	1	330	1.604	11
214	2.080	17			

The thermogravimetric reduction plot of $InSr_3NiO_6$ is shown in Figure 1. The mass loss upon reduction of this phase was 8.9(1)%, corresponding to an oxygen content of 5.97(1) per formula unit. The small plateau at around 1.7% mass loss suggests that Ni^{3+} is initially reduced to Ni^{2+}, before In^{3+} and Ni^{2+} are together reduced to their metallic states.

[*] Dr. J. P. Attfield
Department of Chemistry, University of Cambridge
Lensfield Road, Cambridge CB2 1EW (UK)
and
Interdisciplinary Research Centre in Superconductivity
University of Cambridge, Madingley Road, Cambridge CB3 0HE (UK)
Fax: Int. code +(1223) 336-362
e-mail: jpa14@cam.ac.uk

Dr. M. James
Neutron Scattering Group, ANSTO, Lucas Heights Research Laboratories
Private Mail Bag 1, Menai, N. S. W. 2234 (Australia)

  0947-6539/96/0206-0737 $ 15.00+.25/0

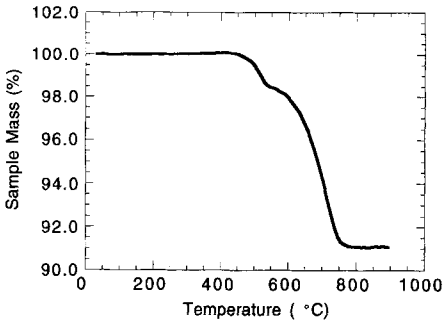

Fig. 1. Thermogravimetric reduction profile for $InSr_3NiO_6$.

Rietveld refinements of the MSr_3NiO_6 structures were carried out on powder X-ray diffraction data. The starting model in space group $R\bar{3}c$ was that previously used for $YbSr_3NiO_6$ [13] and is derived from the structure of Sr_4PtO_6 [14, 15] with M at the unique trigonal prismatic Sr site and Ni at the Pt site (Fig. 2). The impurity phases were also fitted by refining their scale factors and lattice parameters. Variation of the site occupancies

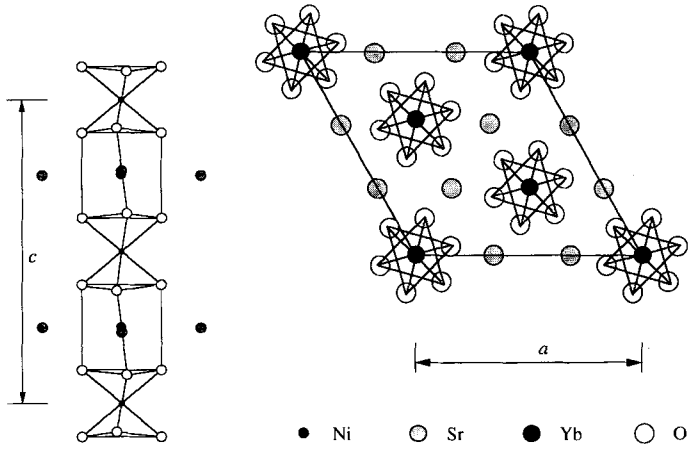

Fig. 2. Left: $NiYbO_6$ chains. Right: unit cell for $YbSr_3NiO_6$.

showed that all the sites are fully occupied in $ScSr_3NiO_6$ and $InSr_3NiO_6$, but for MSr_3NiO_6 with M = Tm, Yb and Lu a deficiency of scattering of about 12% was observed at the M site. In these cases, the observed electron density at the M site is equally consistent with ca. 12% vacancy formation, ca. 18% Ni substitution or ca. 26% Sr substitution. The latter possibility can be discarded as the average "M"–O distance is less then that expected for M alone, whereas Sr substitution would expand this site.

To distinguish between the vacancy formation and Ni substitution models, the structure of $YbSr_3NiO_6$ was refined by using time-of-flight neutron and X-ray powder diffraction profiles simultaneously. In the latter stages of this refinement, Yb and Ni atoms were placed at the M site and their occupation factors were freely refined, giving occupation factors of 0.84(1) and 0.15(1), respectively. The total Yb+Ni occupancy of 0.99(2) does not differ significantly from unity, showing that Ni substitution and not vacancy formation occurs. The total Yb+Ni occupancy was thus constrained to be 1.0 in the final model. There was no evidence for disorder or vacancies at any other site.

The results of the powder X-ray refinements are given in Table 2, and X-ray diffraction profiles of $InSr_3NiO_6$ are shown in Figure 3. The derived variations of c/a and V with M^{3+} ionic

Table 2. Profile and structural parameters, interatomic distances and angles, and impurity phase ratios for MSr_3NiO_6 (M = Sc, In, Lu, Yb and Tm) (e.s.d.'s in parentheses).

	Sc	In	Lu	Yb	Tm
Cell parameters					
a (Å)	9.6595(2)	9.6458(3)	9.6856(2)	9.6851(2)	9.6838(2)
c (Å)	10.8546(3)	11.1111(3)	11.0145(2)	11.0960(2)	11.1193(3)
V (Å^3)	877.10(4)	895.29(6)	899.57(4)	901.37(4)	903.02(5)
R factors (%)					
R_{WP}	4.8	6.5	5.4	2.8	6.7
R_P	2.9	4.2	3.5	1.9	4.4
R_F	4.1	3.5	2.9	4.1	5.5
Atomic parameters [a]					
Ni U_{iso} (Å^2)	0.006(1)	0.002(2)	0.005(1)	0.005(1)	0.008(2)
Sr x	0.3709(1)	0.3705(1)	0.3701(1)	0.3704(1)	0.3698(2)
Sr U_{iso} (Å^2)	0.006(1)	0.007(1)	0.006(1)	0.005(1)	0.008(1)
M U_{iso} (Å^2)	0.001(1)	0.005(1)	0.001(1)	0.005(1)	0.002(1)
M/Ni occup.	1.00	1.00	0.81(1)/0.19	0.83(1)/0.17	0.81(1)/0.19
O x	0.1746(6)	0.1781(6)	0.1759(6)	0.1785(6)	0.1755(8)
O y	0.0220(5)	0.0232(8)	0.0228(7)	0.0249(8)	0.0238(9)
O z	0.1158(3)	0.1140(6)	0.1112(5)	0.1113(6)	0.1108(7)
O U_{iso} (Å^2)	0.002(1)	0.001(2)	0.005(2)	0.008(2)	0.009(2)
Interatomic distances (Å)					
Ni–O × 6	2.028(5)	2.055(6)	2.022(5)	2.039(6)	2.017(7)
M–O × 6	2.157(5)	2.214(6)	2.222(5)	2.235(6)	2.224(7)
Sr–O × 2	2.483(5)	2.489(6)	2.523(5)	2.516(6)	2.534(7)
Sr–O × 2	2.610(5)	2.629(6)	2.603(5)	2.599(6)	2.612(8)
Sr–O × 2	2.649(5)	2.637(6)	2.644(6)	2.629(6)	2.634(8)
Sr–O × 2	2.690(5)	2.696(6)	2.703(6)	2.718(6)	2.714(8)
mean	2.608(5)	2.613(6)	2.618(6)	2.616(6)	2624(8)
Interatomic angles (°) [b]					
O-Ni-O′	85.6(2)	86.0(3)	86.8(2)	87.1(3)	86.6(3)
O-Ni-O″	94.4(2)	94.0(3)	93.2(2)	92.9(3)	93.4(3)

[a] See Table 3 for atomic positions. [b] $z(O) = z(O') = -z(O'')$.

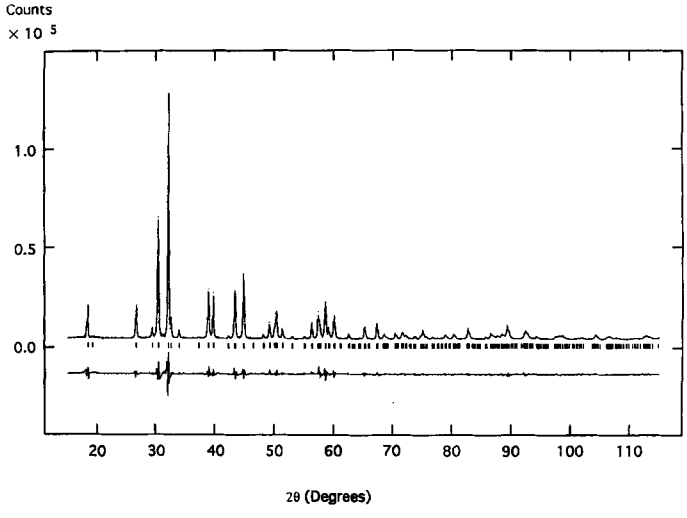

Fig. 3. Observed (points), calculated (full line) and difference X-ray powder diffraction patterns for $InSr_3NiO_6$.

radius are shown in Figure 4, and the twist angles (ϕ) for the distorted MO_6 trigonal prisms (defined in Fig. 5, left) are plotted in Figure 5 (right). The results of the simultaneous refinement of $YbSr_3NiO_6$ are shown in Table 3, and the observed, calculated and difference neutron diffraction profiles are shown in Figure 6. The associated X-ray diffraction profiles are essentially identical to those shown in reference [13].

The molar susceptibility of $YbSr_3NiO_6$ has been previously reported.[13] The magnetisation of MSr_3NiO_6 samples (M = Sc,

0947-6539/96/0206-0738 $ 15.00+.25/0 Chem. Eur. J. 1996, 2, No. 6

Table 3. Profile and structural parameters from the simultaneous refinement of $Yb_{1-x}Ni_xSr_3NiO_6$ from X-ray and TOF neutron diffraction data in space group $R\bar{3}c$ with e.s.d.'s in parentheses (cell dimensions (Å): $a = 9.6831(3)$, $c = 11.0913(3)$).

a) R factors (%).

	R_{WP}	R_P	R_F
X-ray	3.1	2.0	4.2
TOF neutron	2.1	3.6	1.4

b) Atomic parameters.

Atom	Position	x	y	z	U_{iso} (Å^2)	Site occup.
Ni	6*b*	0	0	0	0.0056(2)	1.0
Yb/Ni	6*a*	0	0	0.25	0.0051(2)	0.833(8)/0.167
Sr	18*e*	0.3707(1)	0	0.25	0.0073(1)	1.0
O	36*f*	0.1748(1)	0.0226(1)	0.1106(1)	0.0110(2)	1.0

c) Interatomic distances (Å) and angles (°)

Ni–O	×6	2.0112(5)	Yb/Ni–O	×6	2.2208(4)
Sr–O	×2	2.5408(6)	Sr–O	×2	2.6048(5)
Sr–O	×2	2.6437(5)	Sr–O	×2	2.6971(7)
O-Ni-O′	×6	86.68(2)	O-Ni-O″	×6	93.32(2)
O′-Ni-O″	×3	180.0			

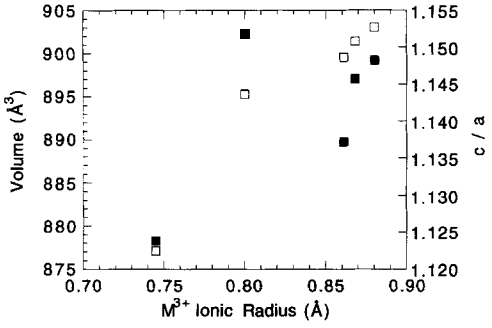

Fig. 4. The variation of cell volume V (open squares) and c/a (filled squares) with M^{3+} ionic radius for MSr_3NiO_6 (M = Sc, In, Lu, Yb and Tm in order of increasing radius).

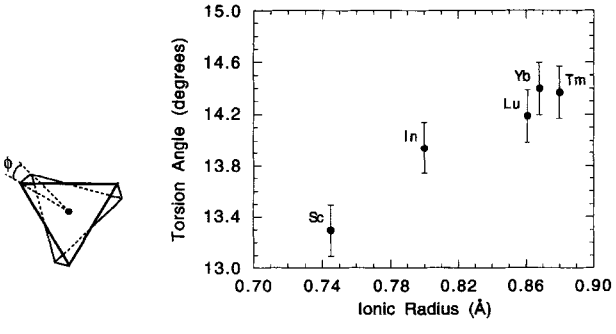

Fig. 5. Left: Schematic diagram of distorted MO_6 trigonal prism defining the twist angle (ϕ). Right: Plot of twist angle versus M^{3+} ionic radius for MSr_3NiO_6.

In and Lu) were initially measured between 6 and 325 K. The inverse molar susceptibilities ($1/\chi_M$), calculated from these data, are shown in Figure 7. $InSr_3NiO_6$ and $LuSr_3NiO_6$ show Curie–Weiss behaviour throughout, whereas $ScSr_3NiO_6$ displays a broad magnetic transition between around 250 and 290 K. To clarify the magnetic behaviour of $ScSr_3NiO_6$ above the anomaly, the susceptibility of a second sample encapsulated by a quartz holder was measured up to 400 K. Effective magnetic moments (μ_{eff}) and Weiss parameters (θ) for the M = In, Yb and Lu phases, and for $ScSr_3NiO_6$ below 200 K and above 300 K are given in Table 4.

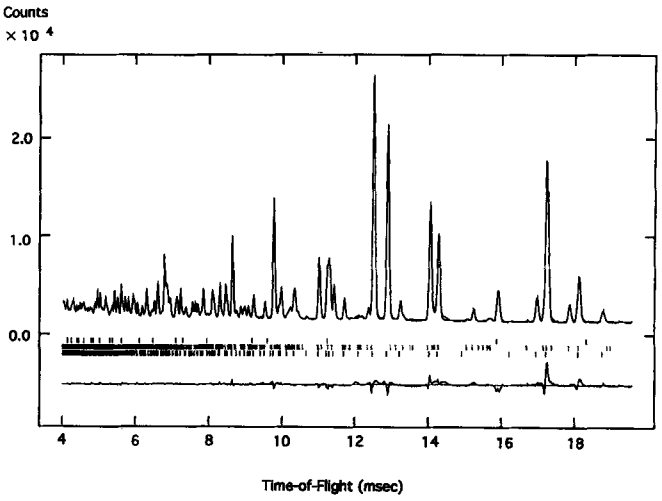

Fig. 6. Observed (points), calculated (full line) and difference time-of-flight neutron powder diffraction patterns for $YbSr_3NiO_6$. Reflection bars for the principal phase and the impurities Yb_2SrO_4 and SrO are shown.

Table 4. Effective moments (μ_{eff}) and Weiss parameters (θ) for MSr_3NiO_6 (M = Yb, Lu, In and Sc) fitted over the given temperature ranges.

M	T (K)	μ_{eff} (B. M.)	θ (K)
Yb	150–300	4.6(1)	−29(1)
Lu	6–300	2.30(1)	3.4(1)
In	6–300	1.97(1)	2.4(1)
Sc (sample 1)	6–200	2.20(1)	3.2(1)
Sc (sample 2)	6–200	2.18(1)	4.4(1)
Sc (sample 2)	300–400	2.11(1)	1.8(1)

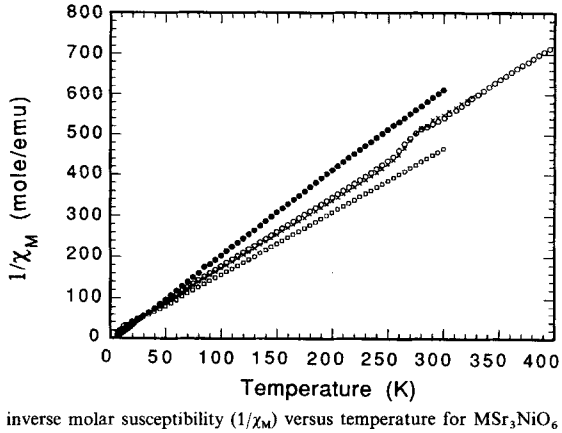

Fig. 7. The inverse molar susceptibility ($1/\chi_M$) versus temperature for MSr_3NiO_6 where M = Sc (two samples; crosses and open circles), In (filled circles) and Lu (open squares).

Discussion

Under the preparative conditions used, rhombohedral K_4CdCl_6-type phases MSr_3NiO_6 are stabilised by a range of M (= Sc, In, Lu, Yb and Tm) at the trigonal prismatic site with ionic radii[21] $r(^{VI}M^{3+})$ between 0.75 and 0.87 Å. Attempts to form these types of phases under the same conditions with M = Ga^{3+} and Er^{3+} (having $r(^{VI}M^{3+}) = 0.62$ and 0.89 Å, respectively), were unsuccessful. The kinetics of formation of these phases also seem to depend upon $r(^{VI}M^{3+})$. The smaller In^{3+} and Sc^{3+} reacted to completion in 20–30 hours, but the larger lanthanide cations took in excess of 150 hours to react with many intermediate regrindings.

Rietveld refinement using X-ray powder diffraction data confirms that MSr_3NiO_6 (M = Sc, In, Lu, and Tm) are isostructural with $YbSr_3NiO_6$ (Fig. 2). In this phase $NiYbO_6$ chains are formed down the threefold z axis by face-sharing between alternating NiO_6 octahedra and slightly twisted YbO_6 trigonal prisms (Fig. 2, left). Strontium, with an irregular eightfold coordination, occupies positions between the $NiYbO_6$ chains (Fig. 2, right). The unit cell volume increases with $r(^{VI}M^{3+})$ (Fig. 4). However, for $InSr_3NiO_6$, a is smaller and c is larger than expected; this is clearly seen in the accompanying plot of c/a .

The simultaneous X-ray and neutron study of $YbSr_3NiO_6$ confirms the oxygen stoichiometry. The ratio of X-ray ($f_{Yb}(0):f_{Ni}(0) = 2.50$) and neutron ($b_{Yb}:b_{Ni} = 1.22$) scattering factors for Yb and Ni are sufficiently different that good contrast was obtained in the simultaneous refinement, enabling the substitution of Ni for Yb to be demonstrated. The M = Tm, Yb and Lu phases are of composition $(M_{1-x}Ni_x)Sr_3NiO_6$ with $x \approx 0.17$, but for M = Sc or In x is 0.

The rhombohedrally distorted NiO_6 octahedra (D_{3d} symmetry) in the MSr_3NiO_6 structures are elongated parallel to c, and the Ni–O bond lengths and angles (Table 2) vary little with M. A similar Ni^{3+} environment is found in $LiNiO_2$,[22] with six equivalent Ni–O distances of 1.969(1) Å, and *cis* O-Ni-O bond angles of 86.1 and 93.9°. The increase in M–O distance on going from M = Sc to Tm is less than would be expected on the basis of their ionic radii. For the larger cations the mean $r(^{VI}M^{3+})$ is reduced by approximately 6% through the substitution of Ni, and by increasing the twist angle of the trigonal pyramid (Fig. 5, right), which enables the triangular faces to approach each other more closely. Less size pressure at the M site for M = Sc and In does not result in any observable Ni substitution.

These compounds are the first $M^{III}Sr_3T^{III}O_6$ oxides (T = transition metal) to be synthesised with the rhombohedral $R\bar{3}c$ symmetry of a K_4CdCl_6-type[23] structure. Previously only $M^{II}Sr_3T^{IV}O_6$ oxides such Sr_4TO_6 (T = Pt, Ir and Rh),[14] Ca_4TO_6 (T = Pt,[24] and Ir[25]) and $Ni^{II}Sr_3Pt^{IV}O_6$[26] have been reported in which T^{IV} occupies the octahedral sites and Sr^{II}, Ca^{II} or Ni^{II}, are present at the trigonal prismatic sites. It is notable that this structure type enables alkaline earth (Sr, Ca), transition metal (Sc, Ni), lanthanide (Tm, Yb, Lu) and main-group (In) cations to be observed in the unusual trigonal-prismatic coordination geometry. An isostructural disordered phase $Cu_{0.75}Ca_{0.25}(Sr_{1.5}Ca_{1.5})PtO_6$ has also been reported,[27] as well as $CuSr_3PtO_6$ and $CuSr_3IrO_6$, which crystallise in the monoclinic subgroup $C2/c$.[28] In these structures, Cu^{II} is displaced from the centre of the trigonal prism towards one of the square faces; this results in a typical CuO_4 square-planar geometry.

Ternary $M^{II}-T^{IV}$ oxides can display the perovskite-type MTO_3, K_2NiF_4-type M_2TO_4 and K_4CdCl_6-type M_4TO_6 structures as the M/T ratio increases. The relationships between these and other hexagonal perovskite structures have recently been described.[29] The same progression of structures may now be generated by the double substitution of Ln^{III} and Ni^{III} for M^{II} and T^{IV} giving $LnNiO_3$, $LnSrNiO_4$ and $LnSr_3NiO_6$. The former two structures are stabilised by large lanthanide cations (Ln = La–Gd), but the latter is stabilised by the cation ordering of small Ln (= Tm–Lu) and Sr cations.

The MSr_3NiO_6 structure provides a good opportunity to study the magnetic properties of Ni^{3+} within isolated NiO_6 octahedra. We have previously shown that when paramagnetic Yb^{3+} is present at the M site a broad maximum is observed at around 12 K, suggesting possible one-dimensional magnetic ordering due to antiferromagnetic superexchange interactions within the $YbNiO_6$ chains.[13] This is supported by the Weiss constant $\theta = -29$ K extracted from the high-temperature region where the magnetic susceptibility follows the Curie–Weiss law. With diamagnetic Sc, In or Lu present in the trigonal prismatic sites between the NiO_6 octahedra, there is no evidence for any short-range magnetic order down to 4 K (Fig. 7), and small values of θ in the range 2–4 K are found. The μ_{eff} values in Table 4 are all characteristic of low-spin $3d^7$ Ni^{3+}; however, the broad transition observed for $ScSr_3NiO_6$ between 250 and 290 K suggests that two subtly different limiting forms of magnetic behaviour are possible for these phases. For $LuSr_3NiO_6$ and $ScSr_3NiO_6$ (<250 K), μ_{eff} and θ have slightly greater values than for $InSr_3NiO_6$ and $ScSr_3NiO_6$ (>290 K). The anomalous c/a ratio for $InSr_3NiO_6$ (Fig. 4) in comparison to those those for the M = Lu, Yb and Tb analogues may also reflect a subtle electronic difference in the behaviour of Ni^{3+} in these materials.

The rhombohedral distortion of the NiO_6 octahedra in the MSr_3NiO_6 structure does not remove the degeneracy of the ^2E_g ground state of Ni^{3+}. This state is prone to a Jahn–Teller distortion, and so the two magnetic behaviours may be identified with statically (<250 K) and dynamically (>290 K) distorted NiO_6 octahedra. In the former case, the small distortions are not ordered within the structure, so that no change of crystal structure is seen. The proposed dynamic-to-static transition in $ScSr_3NiO_6$ is similar to that reported in $K_2PbCu(NO_2)_6$. The Cu^{2+} ESR spectrum of this compound shows a gradual transition over the range 293–273 K.[30, 31] The room-temperature spectrum gave an isotropic g value of 2.10, but at liquid-nitrogen temperatures g was clearly anisotropic with estimated values of $g_\perp = 2.155$ and $g_\parallel = 2.061$, suggesting a freezing-out of the dynamic distortion to give a static one. The equivalent isotropic g value of 2.12 at 80 K is slightly greater than that at 300 K, consistent with the slight increase in μ_{eff} observed for $ScSr_3NiO_6$ on cooling through the transition. Variable-temperature neutron diffraction and ESR studies of $ScSr_3NiO_6$ are under way to clarify the nature of this unusual transition.

Conclusions

This study has shown that rhombohedral, K_4CdCl_6-type, nickel(III) oxides MSr_3NiO_6 are formed for M = Sc, In, Tm, Yb and Lu at 1100 °C. These are the first oxide phases to adopt this structure type with trivalent ions on both the trigonal-prismatic and octahedral sites. Simultaneous refinement of the structure of $YbSr_3NiO_6$ using X-ray and time-of-flight neutron diffraction data shows that approximately 17% Ni is substituted for Yb at the M site. This substitution is also found for M = Tm and Lu and helps to stabilise the structure by reducing the average ionic radius at the M site.

The magnetic susceptibility curve of $YbSr_3NiO_6$ shows evidence of one-dimensional magnetic interactions within the $NiYbO_6$ chains, but this is not seen with diamagnetic M = Sc, In or Lu. The magnetic susceptibility of $ScSr_3NiO_6$ shows an anomaly between 250 and 290 K, with slightly different Curie–Weiss limiting behaviours above and below this temperature region. This transition is consistent with a change from dynamic to static Jahn–Teller distortions of the $Ni^{III}O_6$ octahedra on cooling.

Experimental Procedure

Sample preparation: Polycrystalline samples with bulk composition MSr_3NiO_6 (M = Sc, In, Ga, Lu, Yb, Tm and Er) were synthesised from spectroscopic-grade powders of strontium carbonate, nickel nitrate hexahydrate and the corresponding metal oxide M_2O_3 (M = Lu, Yb, Tm and Er) or nitrate pentahydrate $M(NO_3)_3 \cdot 5H_2O$ (M = Sc, In and Ga). Prior to weighing the lanthanide oxides were preheated to 1000 °C in air to decompose any carbonate material to the oxide. The

0947-6539/96/0206-0740 $ 15.00+.25/0 Chem. Eur. J. 1996, 2, No. 6

powders were dissolved in dilute nitric acid, and an intimate mixture of the metal oxides was formed by decomposition of a citric acid/ethylene glycol gel. The residues were pelleted and sintered in a tube furnace at 1100 °C under flowing oxygen for up to one week with frequent regrinding and repelleting until no further reaction was evident by powder X-ray diffraction. The reaction times for M = Sc and In (20–30 h) were substantially lower than for M = Tm–Lu (ca. 150 h).

Powder Diffraction: Powder X-ray diffraction profiles were recorded on a Philips PW 1710 diffractometer with $Cu_{K\alpha}$ radiation. Data of sufficient quality for structure refinement were collected over $13 \leq 2\theta \leq 113°$, in 0.025° steps, with integration times of 12 s. These structural refinements were carried out by the Rietveld method [32] using the GSAS program [33] and a refined background function.
The time-of-flight (TOF) powder neutron diffraction profile of $YbSr_3NiO_6$ was collected in 3 h on the POLARIS instrument at the Rutherford Appleton Laboratory. The backscattering profile ($135 \leq 2\theta \leq 158°$) was used in a simultaneous Rietveld refinement of the structure with the above X-ray diffraction data. The diffraction pattern of a Si powder standard was used to calibrate the time-of-flight scale.

Thermogravimetric Analysis: Thermogravimetric analysis of a ≈30 mg sample of $InSr_3NiO_6$ was carried out with a Stanton Redcroft STA 1500 simultaneous thermal analyser. The sample was reduced under a 5% hydrogen in nitrogen mixture (flow rate of 58 mL min^{-1}) over a temperature range of 15 to 900 °C at a heating rate of 10 °C min^{-1}.

Magnetic Susceptibility Measurements: Magnetic susceptibilities were measured using a Quantum Design SQUID magnetometer under an applied field of 3.0 T. Samples were cooled down to 6 K in zero field, and the magnetisation was measured while they were warmed up to 400 K.

Acknowledgements: The authors wish to thank Dr. Dolores Marcos and Jon Chapman for their assistance in collecting the time-of-flight powder neutron diffraction pattern of $YbSr_3NiO_6$. M. J. wishes to thank the University of Sydney and Newman College, Melbourne University, for their support.

Received: October 19, 1995 [F 229]

[1] G. Demazeau, A. Marbeuf, M. Pouchard, P. Hagenmuller, *J. Solid State Chem.* **1971**, *3*, 582.
[2] P. Lacorre, J. B. Torrance, J. Pannetier, A. I. Nazall, P. W. Wang, T. C. Huang, *J. Solid State Chem.* **1991**, *91*, 225.
[3] J. B. Torrance, P. Lacorre, A. I. Nazzal, E. J. Asaldo, C. Niedermayer, *Phys. Rev. B* **1992**, *45*, 8209.
[4] J. Gopalakrishnan, G. Colsmann, B. Reuter, *J. Solid State Chem.* **1977**, *22*, 145.
[5] Y. Takeda, R. Kanno, M. Sakano, O. Yamamoto, M. Takano, Y. Bando, H. Akinaga, K. Takita, J. B. Goodenough, *Mater. Res. Bull.* **1990**, *25*, 293.
[6] K. Sreedhar, C. N. Rao, *Mater. Res. Bull.* **1990**, *25*, 1235.
[7] B. W. Arbuckle, K. V. Ramanujachary, Z. Zhang, M. Greenblatt, *J. Solid State Chem.* **1990**, *88*, 278.
[8] Y. Takeda, M. Nishijima, N. Imanishi, R. Kanno, O. Yamamoto, M. Takano, *J. Solid State Chem.* **1992**, *96*, 72.
[9] M. James, J. P. Attfield, *J. Mater. Chem.* in press.
[10] S. C. Chen, K. V. Ramanujachary, M. Greenblatt, *J. Solid State Chem.* **1993**, *105*, 444.
[11] M. James, J. P. Attfield, *J. Solid State Chem.* **1993**, *105*, 287.
[12] M. James, J. P. Attfield, J. Rodriguez-Carvajal, *Chem. Mater.* **1995**, *7*, 1448.
[13] M. James, J. P. Attfield, *J. Mater. Chem.* **1994**, *4*, 575.
[14] J. J. Randall, L. Katz, *Acta. Crystallogr.* **1959**, *12*, 519.
[15] J. J. Randall, R. Ward, *J. Am. Chem. Soc.* **1959**, *81*, 2629.
[16] JCPDS Grant-in-Aid-Report; 1908, D. Pfoertsch, Penn State University, Pennsylvania, USA.
[17] H. Müller-Buschbaum, R. von Schenck, *Z. Anorg. Allg. Chem.* **1970**, *377*, 70.
[18] J. von Wendenburg, A. Henglein, *Z. Naturforsch.* **1964**, *196*, 955.
[19] J. Lee, G. F. Holland, *J. Solid State Chem.* **1991**, *93*, 267.
[20] G. W. Hoffman, J. J. Brown, *J. Inorg. Nucl. Chem.* **1968**, *30*, 63.
[21] R. D. Shannon, *Acta Crystallogr.* **1976**, *A32*, 751.
[22] R. Kanno, H. Kubo, Y. Kawamoto, T. Kamiyama, F. Izumi, Y. Takeda, M. Takano, *J. Solid State Chem.* **1994**, *110*, 216.
[23] G. Bergerhoff, O. Schmitz-Dumont, *Z. Anorg. Allg. Chem.* **1956**, *284*, 10.
[24] C. L. McDaniel, *J. Am. Ceram. Soc.* **1972**, *55*, 426.
[25] C. L. McDaniel, *J. Solid State Chem.* **1972**, *4*, 275.
[26] T. N. Nguyen, D. M. Giaquinta, H.-C. zur Loye, *Chem. Mater.* **1994**, *6*, 1642.
[27] A. B. Bykov, S. F. Radaev, E. A. Gerkinai, L. N. Dem'yanets, B. A. Maximov, O. K. Mel'nikov, *Kristallografiya* **1990**, *35*, 869.
[28] A. P. Wilkinson, A. K. Cheetham, W. Kunnman, A. Kvick, *Eur. J. Solid State Inorg. Chem.* **1991**, *28*, 453.
[29] G. Bergerhoff and O. Schmitz-Dumont, *Z. Anorg. Allg. Chem.* **1956**, *284*, 10.
[30] M. D. Joesten, S. Takagi, P. G. Lenhert, *Inorg. Chem.* **1977**, *16*, 2680.
[31] H. Elliott, B. J. Hathaway, R. C. Slade, *Inorg. Chem.* **1966**, *5*, 669.
[32] H. M. Rieveld, *J. Appl. Crystallogr.* **1969**, *2*, 65.
[33] A. C. Larson, R. B. Von Dreele, Los Alamos National Laboratory Report No. LA-UR-86-748, **1987**.